

NASA Technical Paper 1453



Low-Speed Wind-Tunnel Investigation of Wing Fins as Trailing-Vortex- Alleviation Devices on a Transport Airplane Model

LOAN COPY: RETURN TO
AFWL TECHNICAL LIBRARY
KIRTLAND AFB, N. M.

Delwin R. Croom and G. Thomas Holbrook

JUNE 1979

NASA





NASA Technical Paper 1453

Low-Speed Wind-Tunnel Investigation of Wing Fins as Trailing-Vortex- Alleviation Devices on a Transport Airplane Model

Delwin R. Croom and G. Thomas Holbrook
Langley Research Center
Hampton, Virginia



National Aeronautics
and Space Administration

**Scientific and Technical
Information Branch**

1979

SUMMARY

An investigation was made in the Langley V/STOL tunnel to determine, by the trailing-wing sensor technique, the trailing-vortex-alleviation effectiveness of both a one- and a two-fin configuration (semicircular with a radius of 0.043 semispan) on a jumbo-jet transport airplane model in its landing configuration. The fins were located on the upper surface of the transport model wing along the 30-percent-chord line. The fin configurations were effective in reducing the vortex-induced rolling moment, by amounts varying from 28 to 60 percent, on the trailing wing model located at a distance of 7.8 transport model wing spans downstream of the transport model.

The flow over the fins and over the transport airplane model wing downstream of the fins was observed to be separated and turbulent. All fin configurations caused a reduction in maximum lift coefficient, a positive increment in drag coefficient, and an increment in nose-up pitching-moment coefficient on the transport airplane model.

INTRODUCTION

The strong vortex wakes generated by large transport airplanes are a potential hazard to smaller aircraft. The National Aeronautics and Space Administration is involved in a program of model tests, flight tests, and theoretical studies to investigate aerodynamic means of reducing this hazard. (See ref. 1.)

Results of recent wind-tunnel and water-tank investigations have indicated that the trailing vortices behind a swept-wing transport airplane model can be attenuated by fins of various shapes and planforms when they are located well forward on the upper surface and near the midspan of the transport airplane wing. (See ref. 2.) In these investigations, fins with rectangular, triangular, and semicircular shapes were tested. It was found that semicircular fins provided as much or more alleviation at the same downstream location than either the triangular or rectangular fins having the same planform area. All data reported in reference 2, however, were obtained with the transport airplane model set at only one angle of attack in each of the test facilities (4° in wind-tunnel investigations and 5° in water-tank investigations) with the horizontal-tail incidence angle set at 0° in both test facilities. The difference in model attitude in the two facilities resulted in slightly different lift coefficients and out-of-trim conditions for each fin configuration on the transport airplane model. Also, with these limited data, an assessment of the overall effects of the various fin configurations on the longitudinal aerodynamic characteristics of the transport airplane model would be of a stochastic nature.

The purposes of the present investigation, therefore, were to determine the trailing-vortex-attenuation effectiveness of semicircular fin configurations, in both single and double sets, on the transport airplane model at a trim lift coefficient of 1.2 and also to determine the effects that these fin configurations have on the longitudinal aerodynamic characteristics of the transport airplane model. The direct-measurement technique described in reference 3 was used to obtain trailing-wing rolling-moment data with the trailing wing model at 7.8 transport model wing spans behind the transport airplane model. (For the full-scale transport airplane, 7.8 wing spans represent a downstream distance of 0.25 n. mi.)

SYMBOLS

All data are referenced to the wind axes. The pitching-moment coefficients are referenced to the quarter-chord of the wing mean aerodynamic chord.

b	wing span, m
C_D	drag coefficient, $\frac{\text{Drag}}{qS_W}$
C_L	lift coefficient, $\frac{\text{Lift}}{qS_W}$
$C_{l,TW}$	trailing-wing rolling-moment coefficient, $\frac{\text{Trailing-wing rolling moment}}{qS_{TW}b_{TW}}$
C_m	pitching-moment coefficient, $\frac{\text{Pitching moment}}{qS_W\bar{c}_W}$
c	wing chord, m
\bar{c}	wing mean aerodynamic chord, m
i_t	incidence angle of horizontal tail, referred to fuselage reference line (positive direction trailing edge down), deg
q	free-stream dynamic pressure, Pa
S	wing area, m ²
X',Y',Z'	system of axes originating at left wing tip of transport airplane model (see fig. 1)
x',y',z'	longitudinal, lateral, and vertical dimensions measured from trailing edge of left wing tip of transport airplane model, m

y lateral dimension measured from fuselage reference line, m

α angle of attack of fuselage reference line (wing incidence angle is 2° relative to fuselage reference line), deg

α_f incidence angle of fin relative to undisturbed tunnel flow (positive direction when leading edge toward fuselage) (see fig. 3), deg

Subscripts:

max maximum

trim trim

TW trailing wing model

W transport airplane model

MODEL AND APPARATUS

A three-view sketch and the principal geometric characteristics of the 0.03-scale model of the jumbo-jet transport airplane are shown in figure 1. Figure 2 is a photograph of the transport airplane model mounted on a sting in the Langley V/STOL tunnel. The transport airplane model was the same as that used in the investigation of reference 3. Semicircular fins having both flat-plate and Clark Y airfoil shapes (ref. 4) were tested singularly and in pairs. The fins were pivoted about their center on the 30-percent chord line of the wing. Figure 3 is a sketch showing the details and locations of the fins on the transport model. The fins for the one-fin configurations were located at $0.38b/2$, $0.42b/2$, and $0.46b/2$. The fins for the two-fin configurations were at $0.42b/2$ and $0.50b/2$ and at $0.46b/2$ and $0.53b/2$. Photographs of the fin configurations are presented as figure 4.

A photograph along with the dimensions of the unswept trailing wing model installed on the traverse mechanism is presented in figure 5. The trailing wing model had a span and aspect ratio typical of small-size transport airplanes.

The test section of the Langley V/STOL tunnel has a height of 4.42 m, a width of 6.63 m, and a length of 14.24 m. The transport airplane model was sting supported near the forward end of the tunnel test section on a six-component strain-gage balance system which measured the forces and moments. The angle of attack of the transport model was determined from an accelerometer mounted in the fuselage. The trailing wing model was mounted on a single-component strain-gage roll balance which was attached to a traverse mechanism capable of moving the model both laterally and vertically. (See figs. 2 and 5.) The lateral and vertical positions of the trailing wing model were measured by outputs from digital encoders. The entire traverse mechanism, which could be mounted to the tunnel floor at various tunnel longitudinal positions downstream of the transport airplane model, was located at only one downstream position for these tests.

TESTS AND CORRECTIONS

Transport Airplane Model

The free-stream dynamic pressure in the tunnel test section for all tests was 430.9 Pa which corresponds to a velocity of 26.5 m/sec. The Reynolds number for the tests was approximately 4.7×10^5 based on the wing mean aerodynamic chord. Transition strips approximately 0.30 cm wide of No. 60 abrasive grit were placed 2.54 cm behind the leading edge of the wing; natural transition was used elsewhere. The basic longitudinal aerodynamic characteristics were obtained over a range of angle of attack from approximately -4° to 24° . All tests were made with leading-edge devices extended, landing gear down, and landing flaps deflected to 30° . (See ref. 1.)

Blockage corrections were applied to the data by the method of reference 5. Jet-boundary corrections were applied to the angle of attack and the drag in accordance with reference 6.

Trailing Wing Model

The trailing wing model together with its associated roll-balance system was used as a sensor to measure the vortex-induced rolling moment caused by the vortex flow downstream of the transport airplane model. No transition grit was applied to the trailing model. The trailing model was positioned near the aft end of the tunnel test section (7.8 transport-model wing spans behind the transport airplane model), and the traverse mechanism was positioned laterally and vertically so that the trailing vortex was near the center of the mechanism. The trailing vortex was probed with the trailing model. A large number of trailing-wing rolling-moment data points (usually from 50 to 100) were obtained from the lateral traverses at several vertical locations to ensure good definition of the vortex wake so that the maximum trailing-wing rolling moment could be determined. In addition, certain test conditions were repeated at selected intervals during the test period, and the data were found to be repeatable. All trailing-wing rolling-moment data were obtained with the transport airplane model at a trim lift coefficient of 1.2 ($C_{L,trim} = 1.2$).

RESULTS AND DISCUSSION

Transport Airplane Model

Figures 6 to 11 present the longitudinal aerodynamic characteristics of the transport airplane model with both the one- and two-semicircular-fin configurations positioned along the 30-percent-chord line of each wing panel at several spanwise locations and for several fin incidence angles. Figures 6, 7, 8, and 9 (with $i_t = 0^\circ$) show that for any of the one-fin configurations, at a lift coefficient of 1.2, there is a penalty in drag coefficient of about 0.02. Also, an increase of about 0.5° to 0.75° in angle of attack of the transport airplane model is required to maintain a lift coefficient of 1.2. The data in figure 9 indicate that there is no advantage of the Clark Y airfoil fin over the flat-plate airfoil fin at a fin incidence angle of 36° .

For the two-fin configurations with $i_t = 0^\circ$ (figs. 10 and 11) the penalty in drag coefficient, at a lift coefficient of 1.2, varies from about 0.04 at fin incidence angles of 24° to about 0.06 at fin incidence angles of 36° . Correspondingly, for the two-fin configurations, an increase in angle of attack of the transport airplane model of from about 0.75° to 1.50° is required to maintain a lift coefficient of 1.2. All the fin configurations investigated caused a reduction in maximum lift coefficient. (See figs. 6 to 11.) These data also show that all the fin configurations gave a positive increment in nose-up pitching-moment coefficient and that the linear range of pitching-moment coefficient generally was extended to a higher angle of attack.

Based on the discussion presented in reference 2, it was anticipated that the overall flow over the wing would be improved by the fins. However, during this investigation, observations made of tufts installed on the fins and on the wing and flaps behind the fins showed that the flow was separated and turbulent over the fin and downstream of the fin. These observations indicated that there was an area on the wing downstream of the fins over which the lift was reduced. This reduction in lift, therefore, required an increase in angle of attack of the transport airplane model to maintain a given lift coefficient. This separated condition could contribute to the positive increment in nose-up pitching-moment coefficient obtained for all the fin configurations.

Table I presents the angle of attack, horizontal-tail incidence angle, and measured drag coefficient for each of the fin configurations at a trim lift coefficient of 1.2 ($C_{L,trim} = 1.2$). For the trimmed conditions, the angle-of-attack changes and the drag penalties due to the fins are slightly smaller than indicated by the data for the transport airplane model with the horizontal tail set at an incidence angle of 0° . (See figs. 6 to 11.) For fin incidence angles from 24° to 36° , the increase in angle of attack required to maintain a trim lift coefficient of 1.2 varied from about 0° to 0.3° for the one-fin configurations and from about 0° to 1.3° for the two-fin configurations. The drag coefficient penalty was about 0.02 for the one-fin configurations and varied from about 0.03 to 0.06 for the two-fin configurations.

Trailing Wing Model

The maximum rolling-moment coefficient measured by the trailing wing model and the position of this model relative to the left wing tip of the transport airplane model are presented in figure 12 as a function of fin spanwise location for a one-fin (Clark Y airfoil) configuration. These data indicate that the effectiveness of the fin in reducing the induced rolling moment on the trailing model is dependent on fin spanwise location; the largest reduction was realized when the fin was located at the 42-percent semispan location. In reference 2, the largest reduction was also shown to occur with the fin at the 42-percent semispan location.

The maximum rolling-moment coefficient measured by the trailing wing model and the position of this model relative to the left wing tip of the transport airplane model are presented in figure 13 as a function of fin incidence angles for all fin configurations. These measurements were made with transport airplane model at a trim lift coefficient of 1.2. Generally, the figure shows

that, over the range of fin incidence angle from 24° to 36° , the fins reduce the induced rolling-moment coefficient on the trailing wing model as the fin incidence angle is increased. This result is similar to the result in reference 2. The only data point obtained at a fin incidence angle greater than 36° was that for the flat-plate fin at an incidence angle of 90° . The reduction in trailing-wing rolling-moment coefficient with the flat-plate fin at an incidence angle of 90° was about 20 percent less than when the fin incidence angle was 36° . For a one-fin configuration, the maximum reduction in induced rolling moment measured on the trailing model was about 50 percent; for a two-fin configuration, the maximum reduction was about 60 percent. These results are similar to those in reference 2. Figure 13 also shows that, at a fin incidence angle of 36° , a fin with a flat-plate airfoil section was essentially as effective in reducing the induced rolling moment on the trailing model as was a fin with a Clark Y airfoil section.

A summary of the trailing-wing rolling-moment data and the associated penalties in drag and maximum lift of the transport model for all fin configurations is presented in figure 14. The rolling-moment and drag data were obtained with the transport model at a trim lift coefficient of 1.2. The values of $C_{L,max}$ were obtained with the horizontal tail set at 0° . Figure 14 shows that, for all the fin configurations, the maximum lift coefficient of the transport model is reduced as the fin incidence angle is increased, with the largest reductions in lift coefficient being for the two-fin configurations. For the one-fin configurations, the increase in drag coefficient was about 0.02 throughout the range of fin incidence angle from 24° to 36° ; whereas, for the two-fin configurations, the drag coefficient increment increased from about 0.03 to 0.06 as the fin incidence angle increased from 24° to 36° .

SUMMARY OF RESULTS

Results have been presented of an investigation made in the Langley V/STOL tunnel to determine, by the trailing-wing sensor technique, the trailing-vortex-alleviation effectiveness of both a one- and a two-fin configuration (semi-circular with radius of 0.043 semispan) on the wing of a transport airplane model at various spanwise locations and incidence angles. An assessment was also made of the drag and lift penalties of these devices on the transport airplane model.

Results from tests of a one-fin configuration made at spanwise locations of 0.38 semispan, 0.42 semispan, and 0.46 semispan indicated that the largest reduction in induced rolling moment on the trailing wing model was realized when the fin was located at 0.42 semispan.

All fin configurations investigated reduced the induced rolling moment on the trailing wing model. The largest reductions were realized at a fin incidence angle of 36° for both the one-fin configuration (reduction of about 50 percent) and the two-fin configuration (reduction of about 60 percent).

Observations of tufts on the fin and wing of the transport airplane model indicated that the flow over the fins and over the transport airplane model wing downstream of the fins was separated and turbulent.

The results of this investigation indicate that, at fin incidence angles from 24° to 36° , all fin configurations caused a reduction in maximum lift coefficient, an increase in drag coefficient, and a positive increment in nose-up pitching-moment coefficient on the transport airplane model. The increase in drag coefficient was about 0.02 for the one-fin configuration throughout the test range of fin incidence angles. The increase in drag coefficient for the two-fin configuration varied from about 0.03 to 0.06 for fin incidence angles of 24° to 36° , respectively.

Langley Research Center
National Aeronautics and Space Administration
Hampton, VA 23665
May 11, 1979

REFERENCES

1. Wake Vortex Minimization. NASA SP-409, 1977.
2. Rossow, Vernon J.: Experimental Investigation of Wing Fin Configurations for Alleviation of Vortex Wakes of Aircraft. NASA TM-78520, 1978.
3. Croom, Delwin R.; and Dunham, R. Earl, Jr.: Low-Speed Wind-Tunnel Investigation of Span Load Alteration, Forward-Located Spoilers, and Splines as Trailing-Vortex-Hazard Alleviation Devices on a Transport Aircraft Model. NASA TN D-8133, 1975.
4. Pinkerton, Robert M.; and Greenberg, Harry: Aerodynamic Characteristics of a Large Number of Airfoils Tested in the Variable-Density Wind Tunnel. NACA Rep. No. 628, 1938.
5. Herriot, John G.: Blockage Corrections for Three-Dimensional-Flow Closed-Throat Wind Tunnels, With Consideration of the Effect of Compressibility. NACA Rep. 995, 1950. (Supersedes NACA RM A7B28.)
6. Gillis, Clarence L.; Polhamus, Edward C.; and Gray, Joseph L., Jr.: Charts for Determining Jet-Boundary Corrections for Complete Models in 7- by 10-Foot Closed Rectangular Wind Tunnels. NACA WR L-123, 1945. (Formerly NACA ARR L5G31.)

TABLE I.- ANGLE OF ATTACK, DRAG COEFFICIENT, AND HORIZONTAL-TAIL

INCIDENCE ANGLE FOR FIN CONFIGURATIONS AT $C_{L,trim} = 1.2$

Spanwise location of fin	Fin airfoil section	Fin incidence angle, α_f , deg	α , deg	C_D	i_t , deg
Fins off	Fins off	Fins off	2.79	0.218	-2.0
0.38b/2	Clark Y	30	2.78	.233	-1.4
.42b/2	Clark Y	24	3.11	.233	-1.0
.42b/2	Clark Y	30	3.13	.235	-.8
.42b/2	Clark Y	36	2.98	.235	-.8
.42b/2	Flat plate	36	3.13	.234	-2.0
.42b/2	Flat plate	90	3.74	.247	-2.0
.46b/2	Clark Y	24	2.96	.235	-1.0
.46b/2	Clark Y	30	2.80	.236	-1.2
.42b/2 and .50b/2	Clark Y	24	2.70	.244	0
.42b/2 and .50b/2	Clark Y	30	3.78	.268	0
.46b/2 and .53b/2	Clark Y	24	3.18	.256	0
.46b/2 and .53b/2	Clark Y	30	3.39	.268	.2
.46b/2 and .53b/2	Clark Y	36	4.05	.274	-.5

Wing

Span, m	1.79
Mean aerodynamic chord, m	0.25
Root chord, m	0.497
Tip chord, m	0.121
Sweepback at quarter chord, deg	37.5
Area, m ²	0.460
Aspect ratio	6.96

Fuselage

Length, m	2.06
-----------	------

Horizontal tail

Span, m	0.664
Area, m ²	0.123
Aspect ratio	3.6

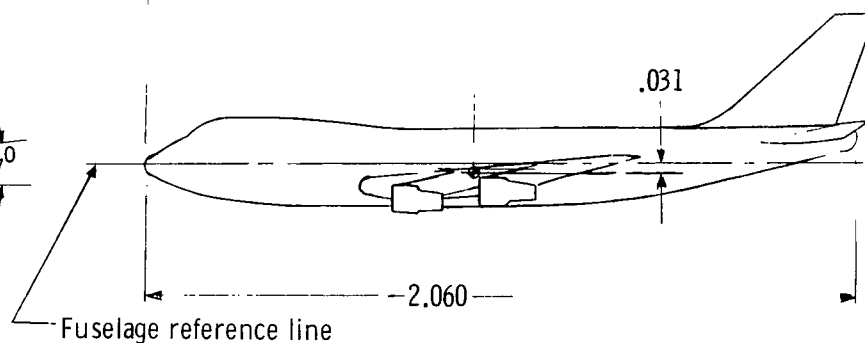
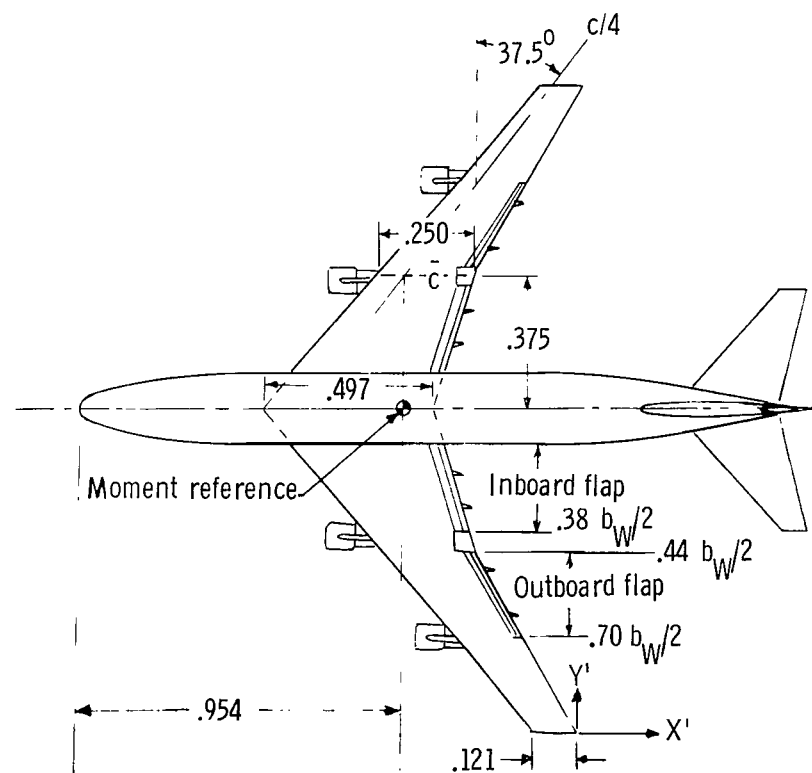
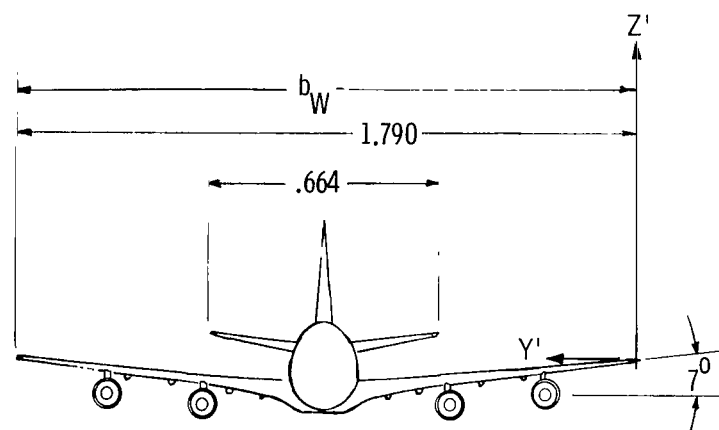


Figure 1.- Three-view sketch of 0.03-scale transport airplane model with flaps and gear retracted. Linear dimensions are in meters.



L-78-3587

Figure 2.- Transport airplane model in the Langley V/STOL tunnel. (Traverse frame for trailing wing model is also shown.)

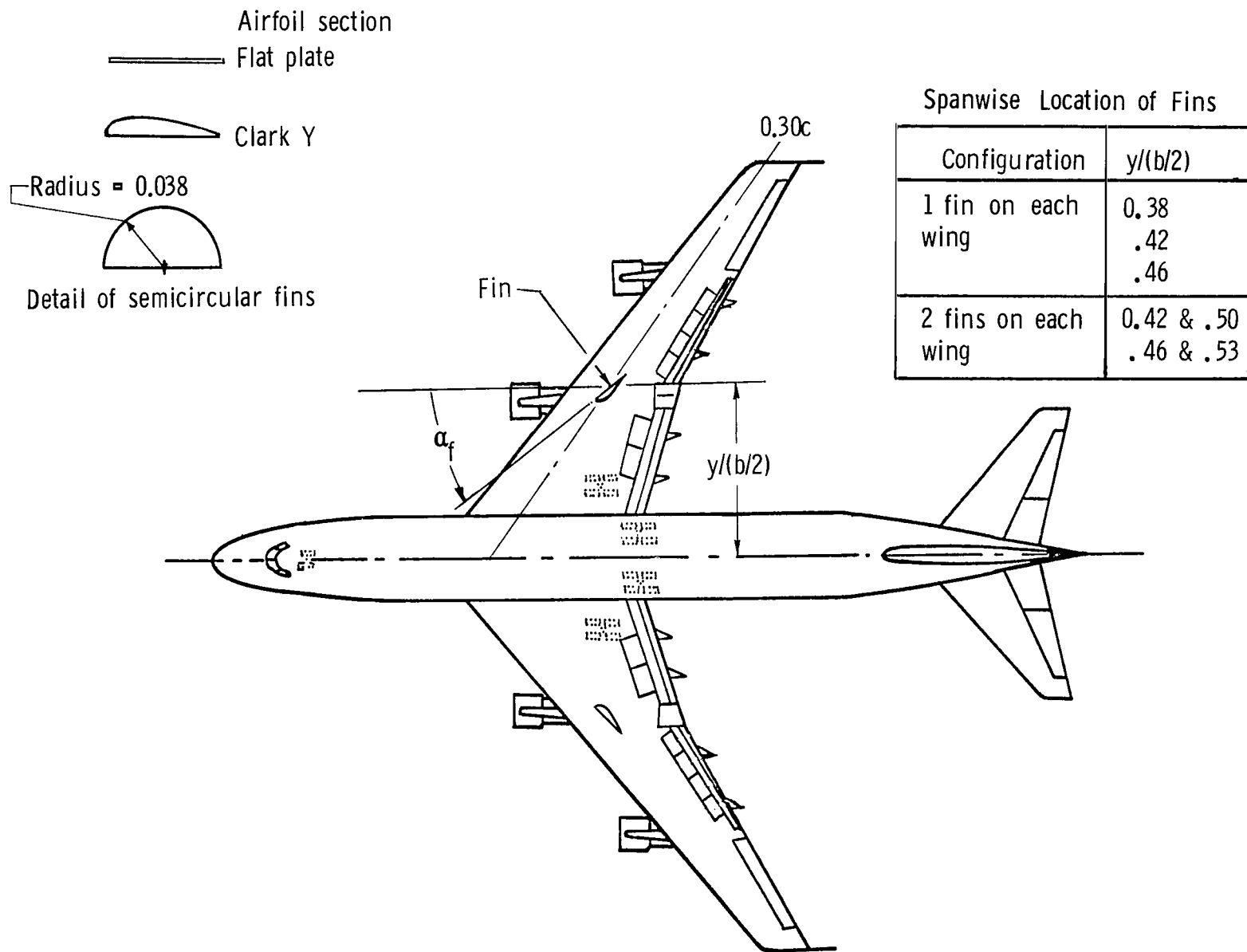
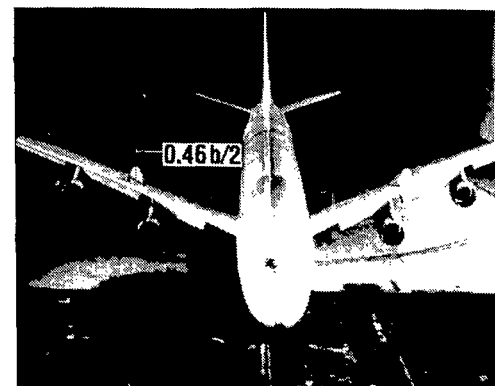
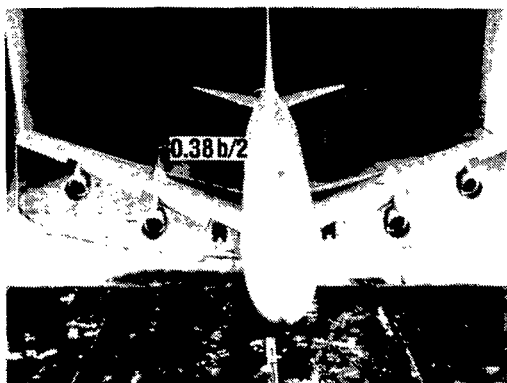
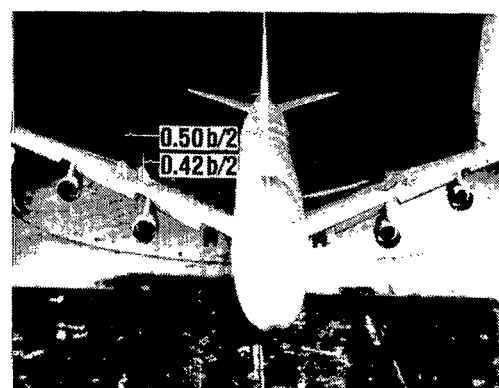


Figure 3.- Sketch of fins on transport airplane model. Linear dimensions are in meters.



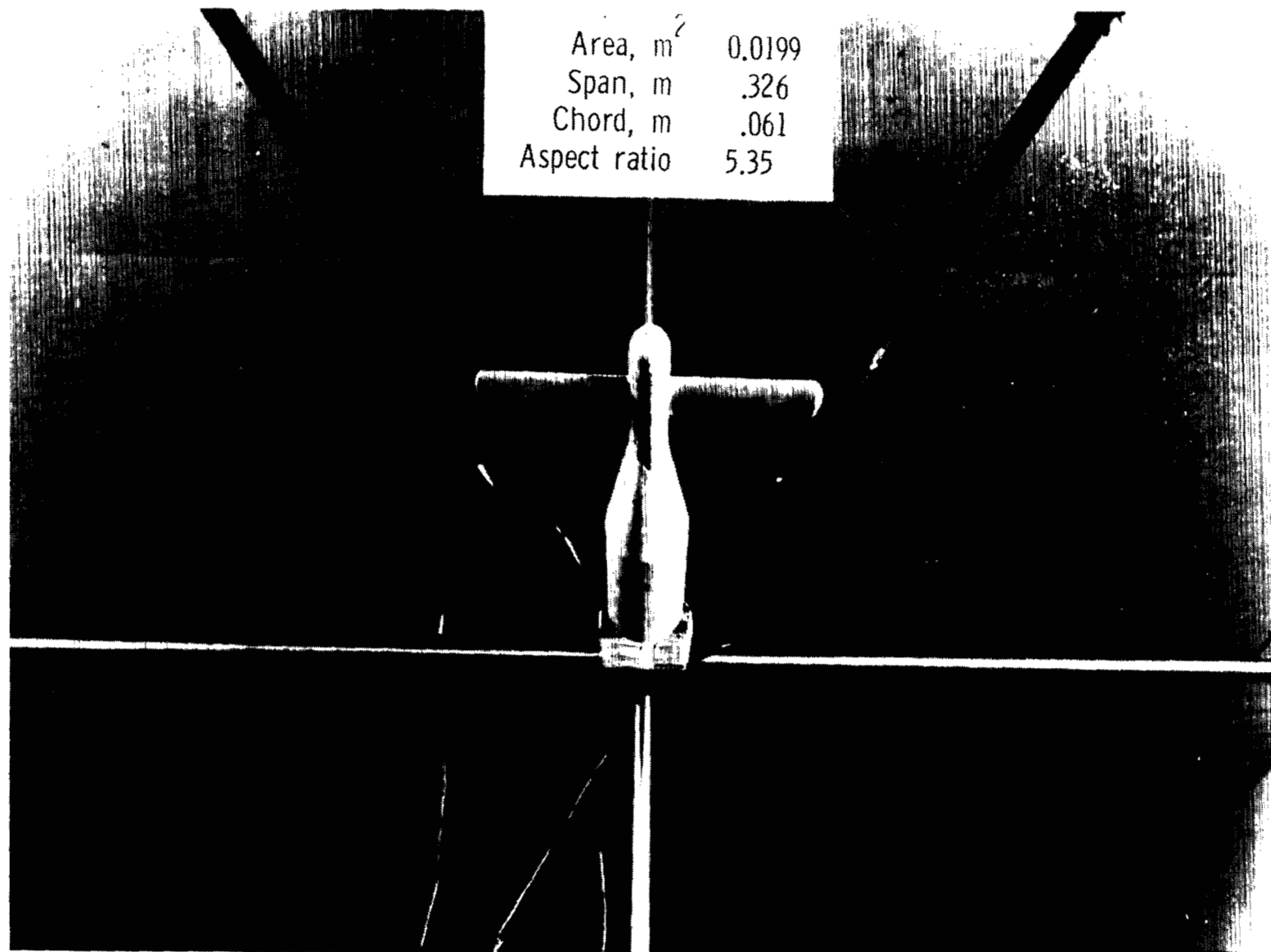
(a) One fin on each wing.



(b) Two fins on each wing.

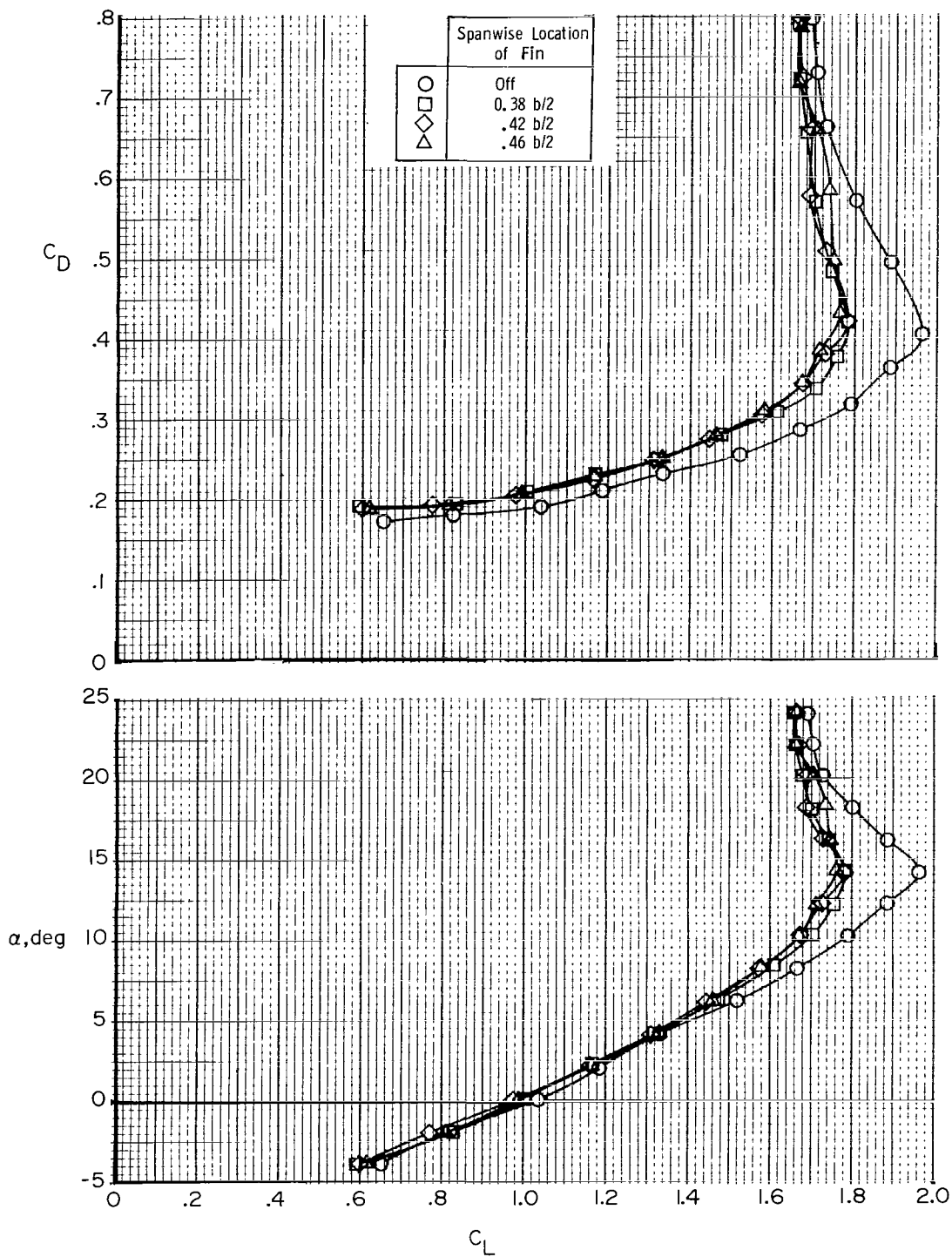
L-79-165

Figure 4.- Fins on transport airplane model.



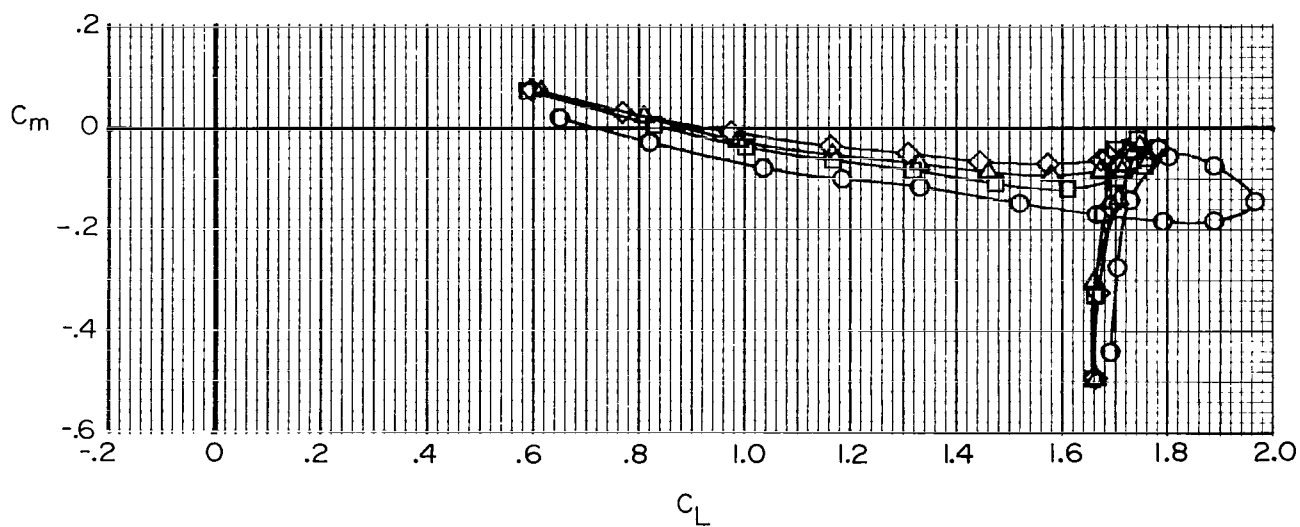
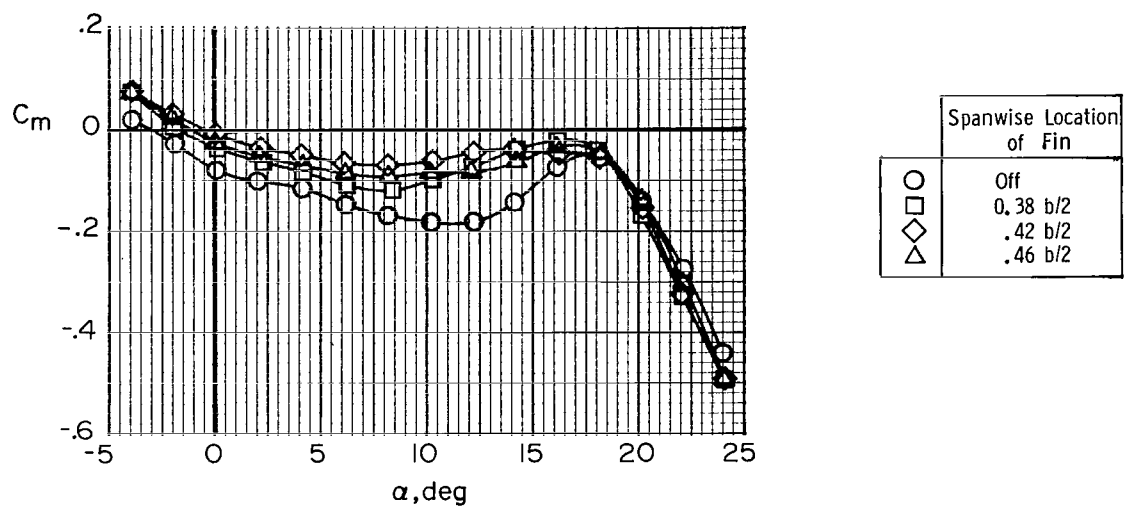
L-75-2411.2

Figure 5.- Unswept trailing wing model on traverse mechanism (looking up at model from point slightly in front of traverse frame). Model has NACA 0012 airfoil section.



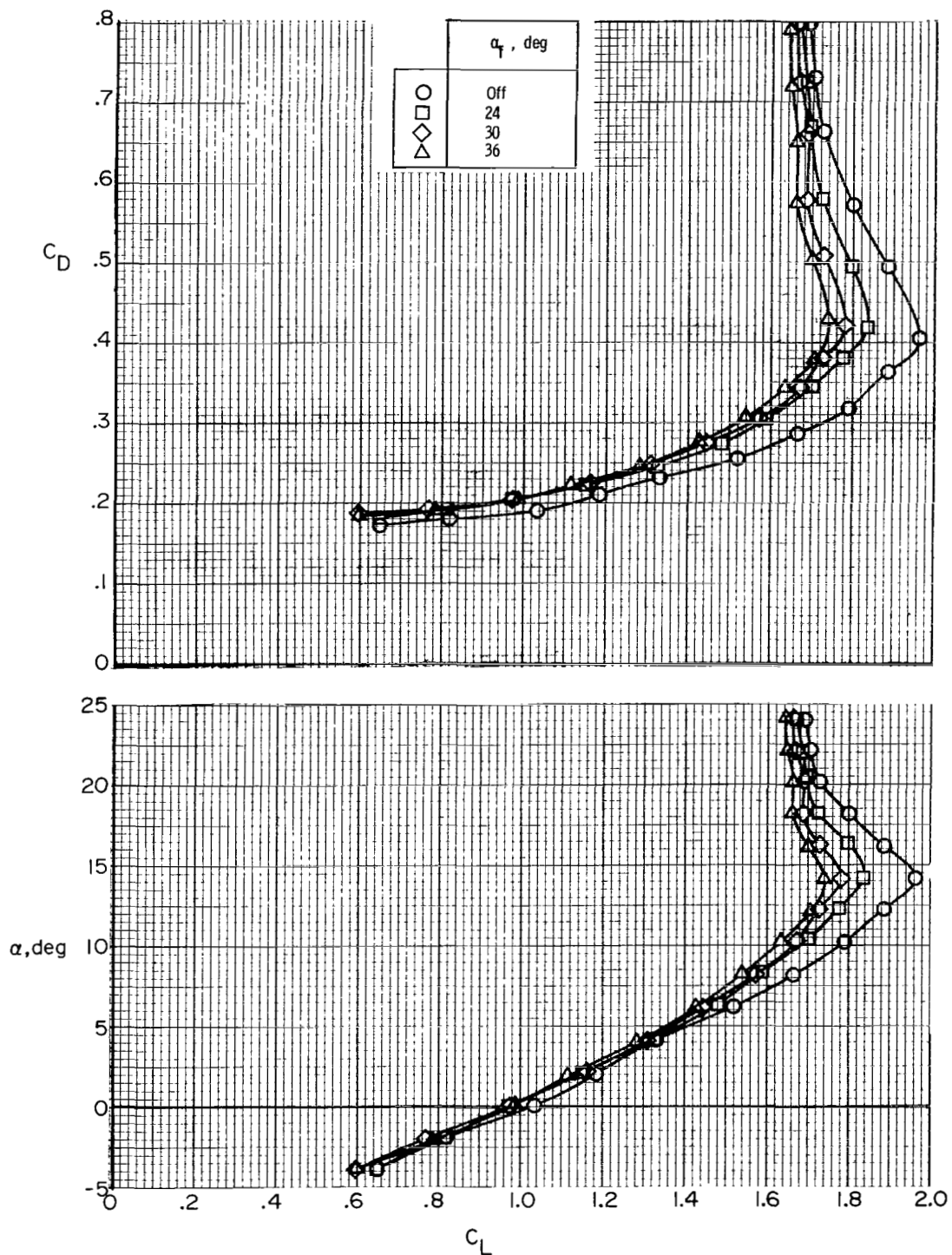
(a) Lift and drag coefficients.

Figure 6.- Effect of spanwise location of one fin on longitudinal aerodynamic characteristics of the transport airplane model with the Clark Y airfoil fin located along 30-percent-chord line at $\alpha_f = 30^\circ$. $i_t = 0^\circ$; landing flap configuration.



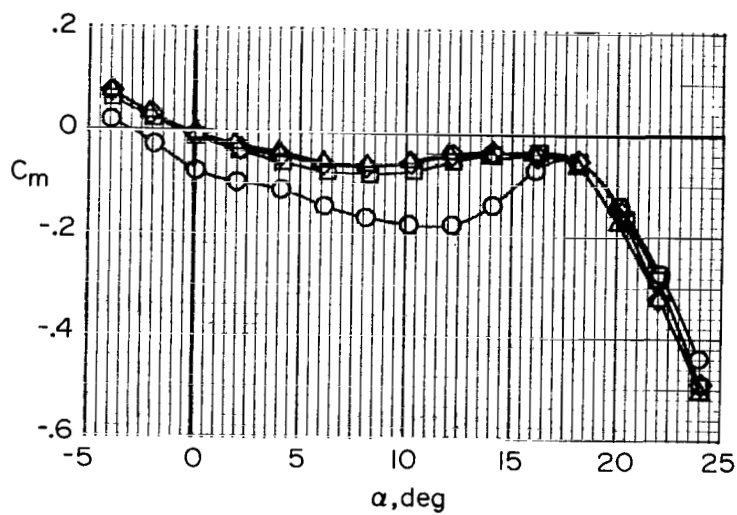
(b) Pitching-moment coefficient.

Figure 6.- Concluded.

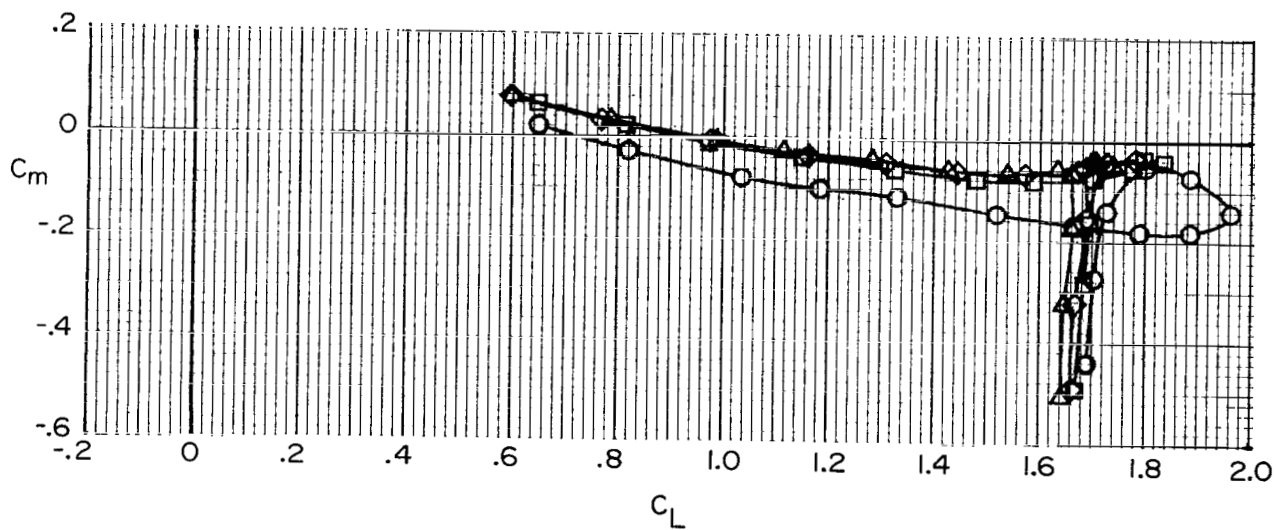


(a) Lift and drag coefficients.

Figure 7.- Effect of α_f of one fin on longitudinal aerodynamic characteristics of the transport airplane model with the Clark Y airfoil fin located along 30-percent-chord line at $0.42b/2$. $i_t = 0^\circ$; landing flap configuration; landing gear down.

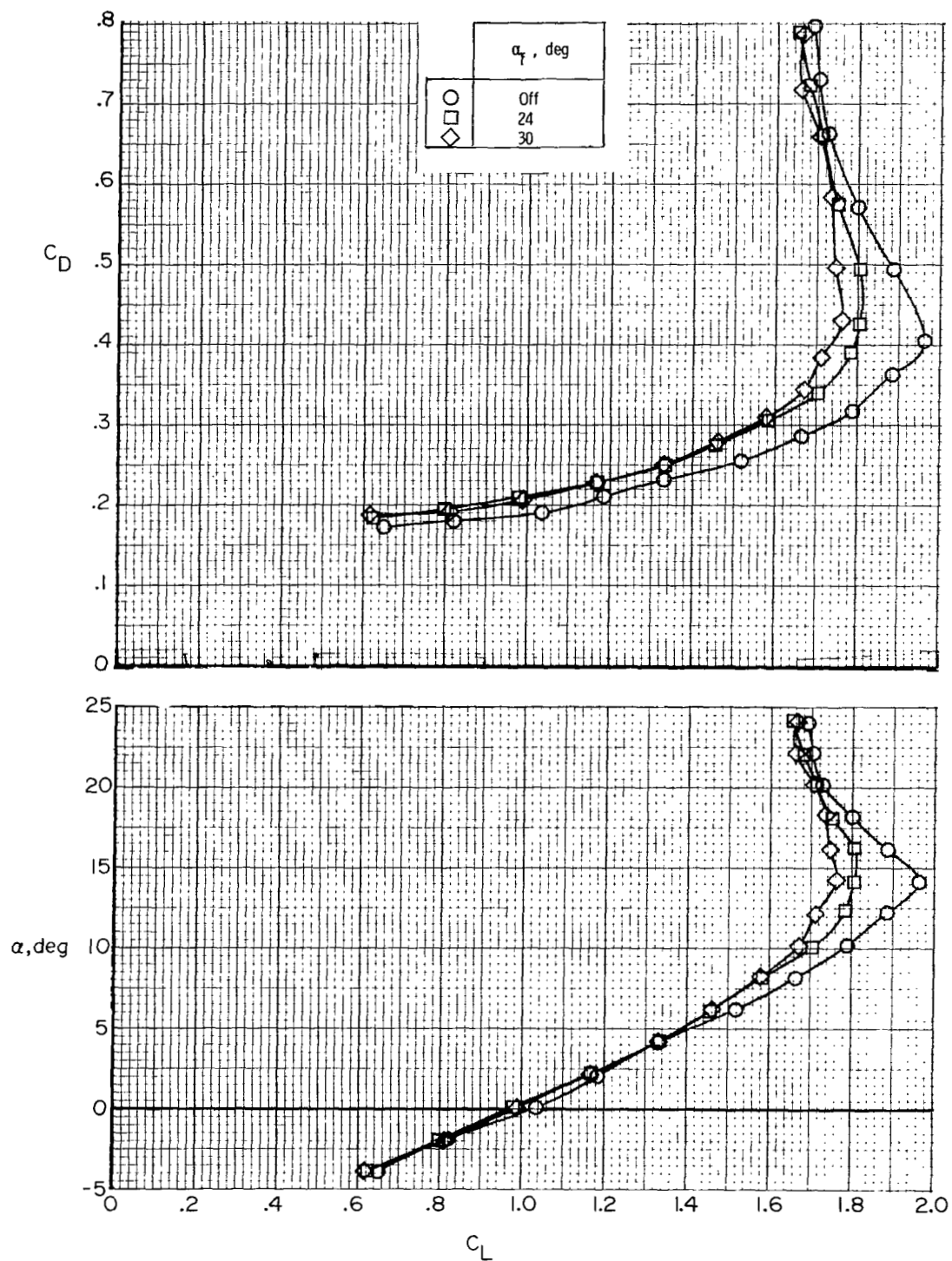


	α_f , deg
○	Off
□	24
◇	30
△	36



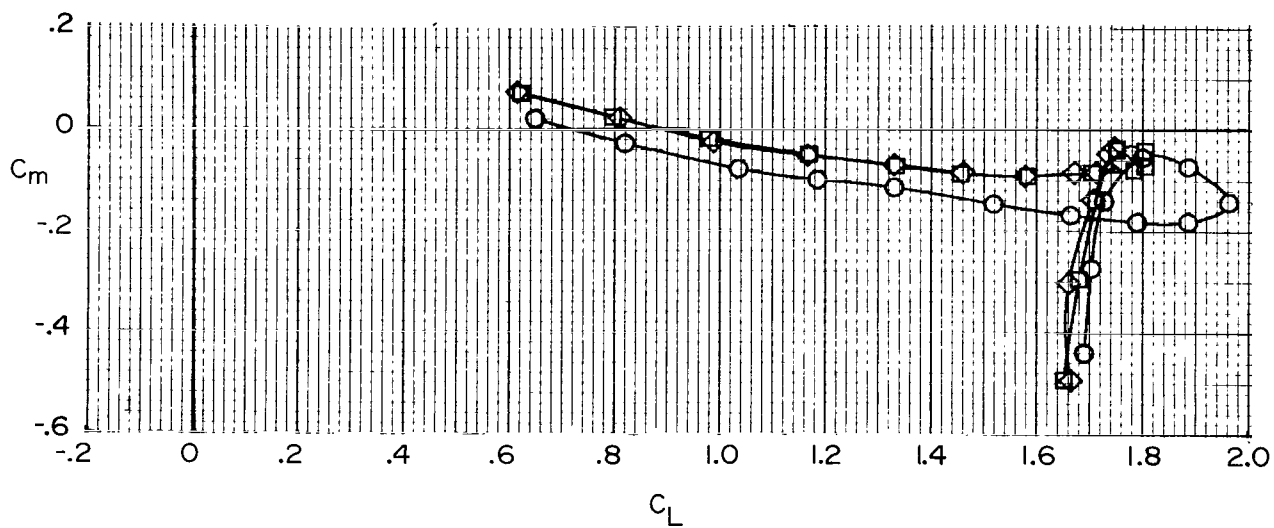
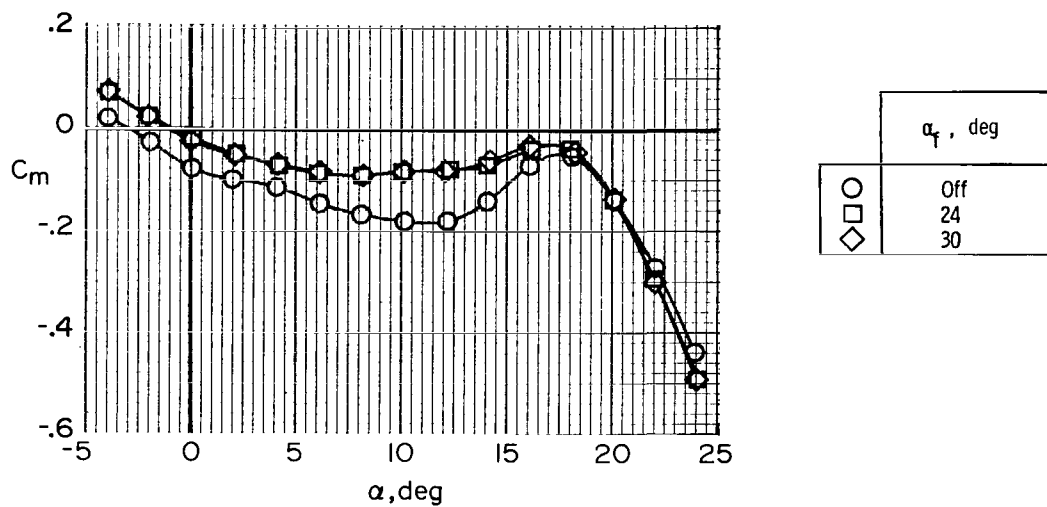
(b) Pitching-moment coefficient.

Figure 7.- Concluded.



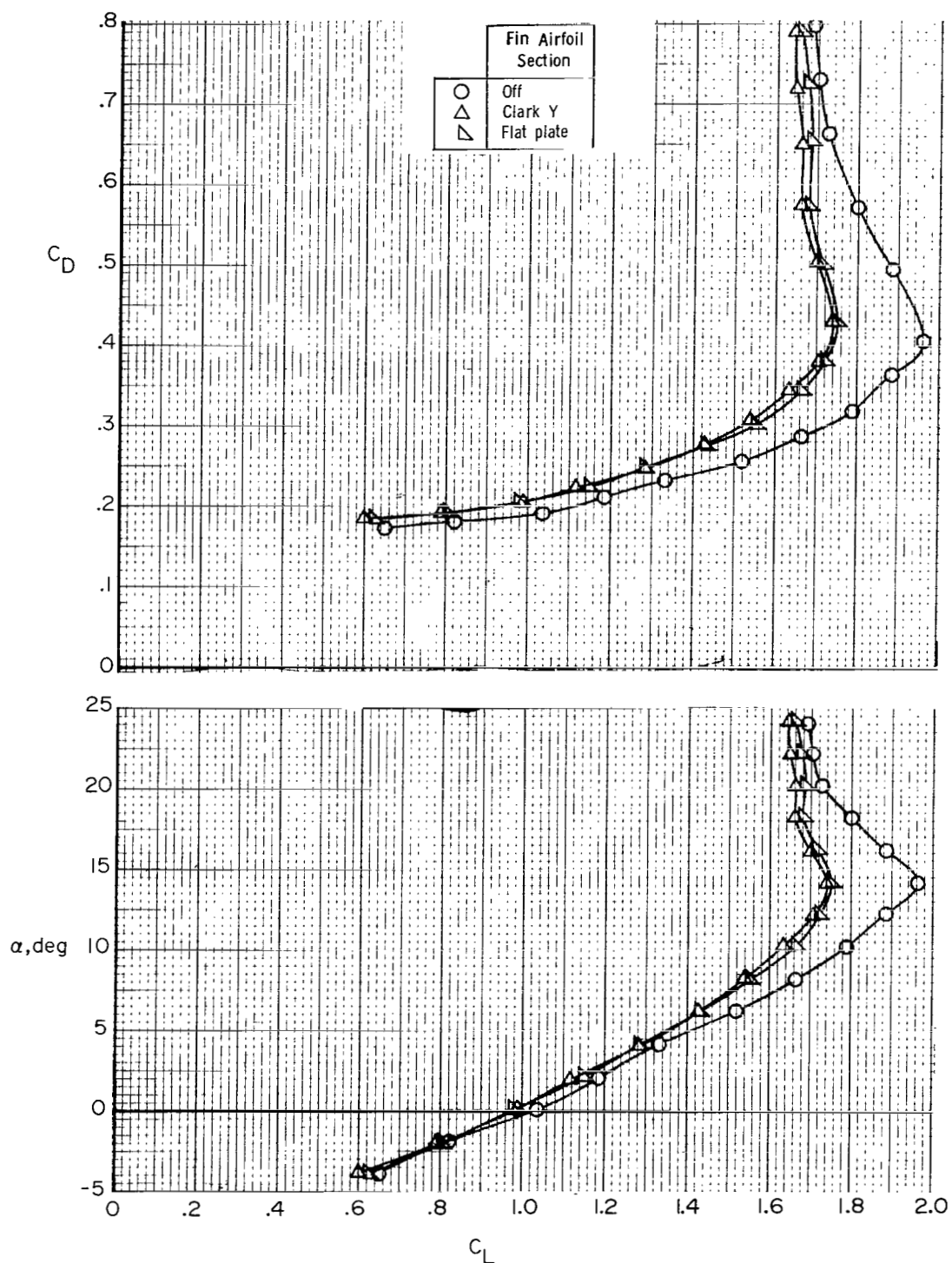
(a) Lift and drag coefficients.

Figure 8.- Effect of α_f of one fin on longitudinal aerodynamic characteristics of transport airplane model with the Clark Y airfoil fin located along 30-percent-chord line at $0.46b/2$. $i_t = 0^\circ$; landing flap configuration; landing gear down.



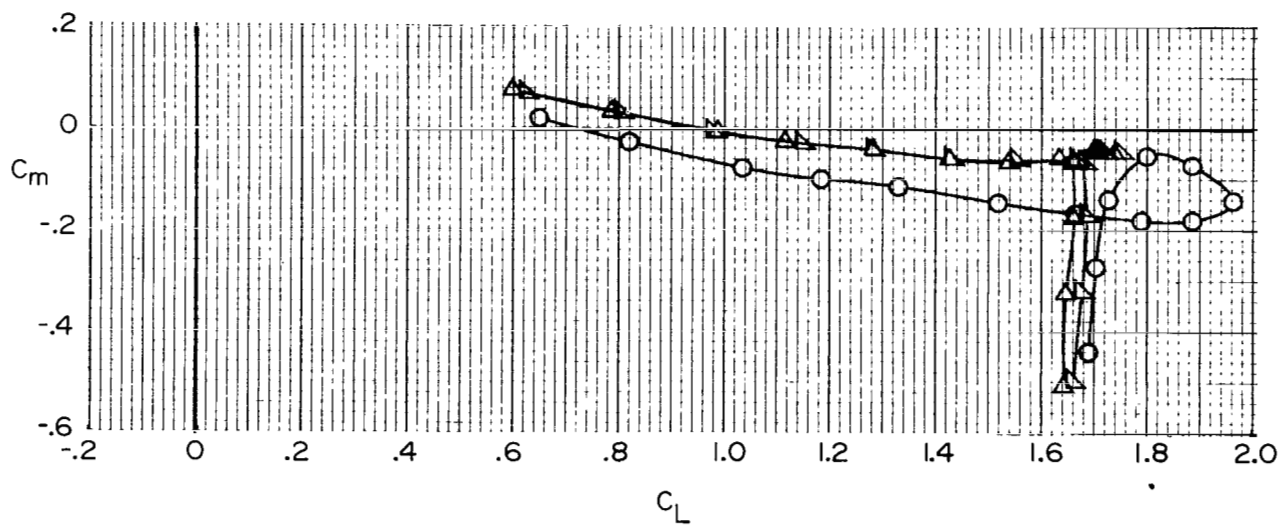
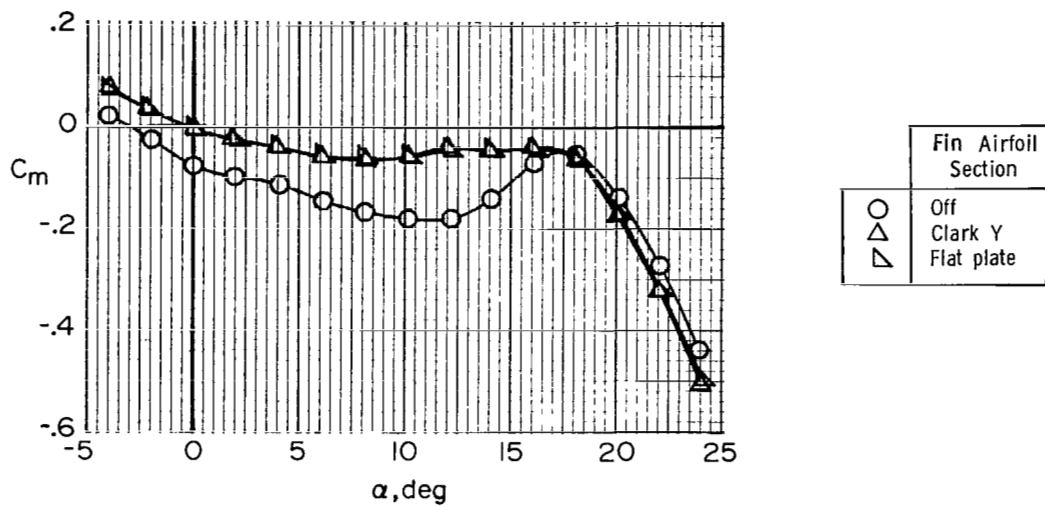
(b) Pitching-moment coefficient.

Figure 8.- Concluded.



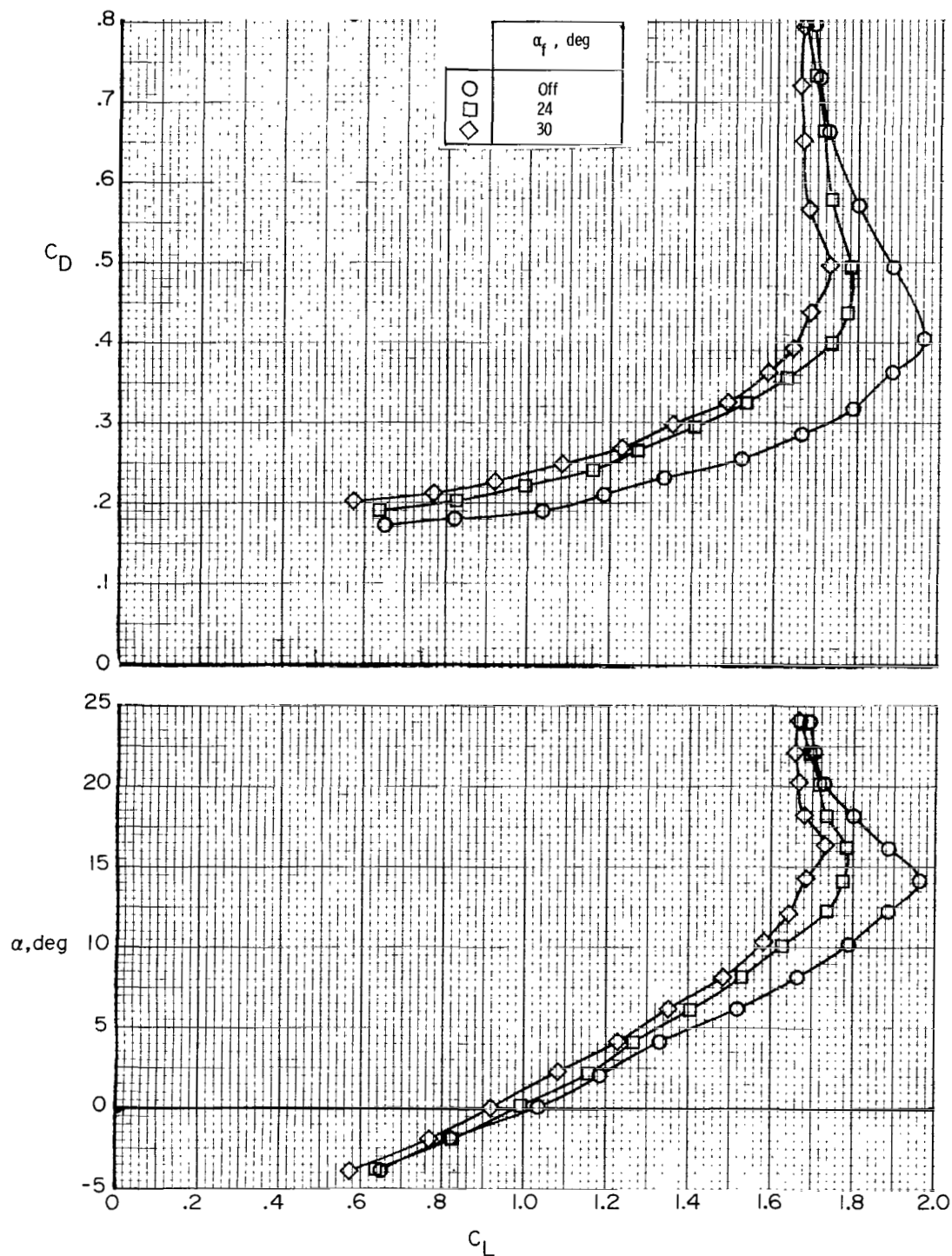
(a) Lift and drag coefficients.

Figure 9.- Effect of airfoil section of one fin on longitudinal aerodynamic characteristics of transport airplane model with the fin located along 30-percent-chord line at $0.42b/2$; $\alpha_f = 36^\circ$. $i_t = 0^\circ$; landing flap configuration; landing gear down.



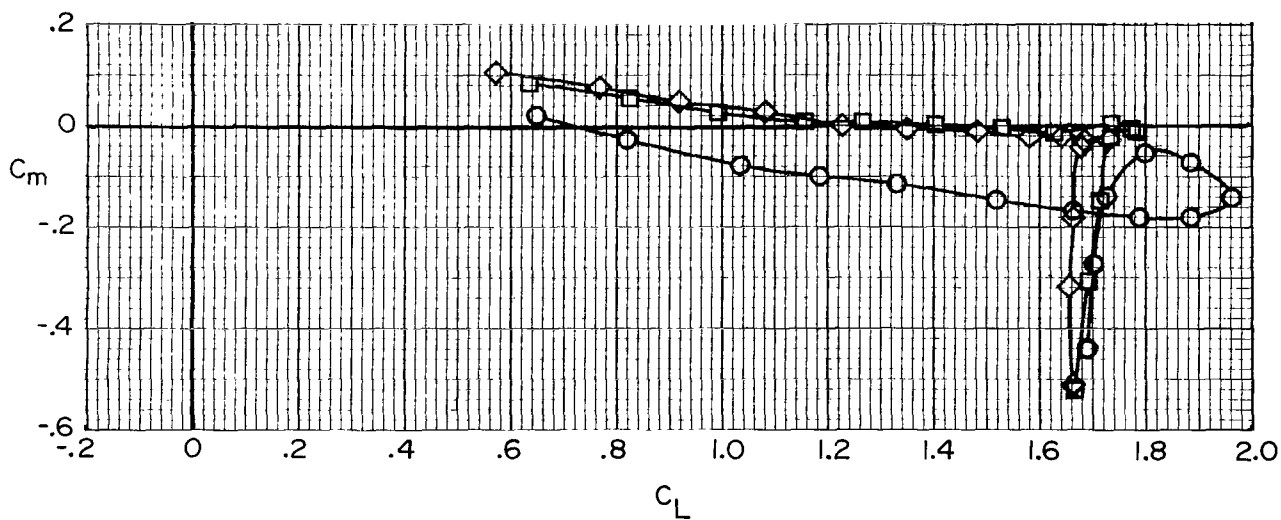
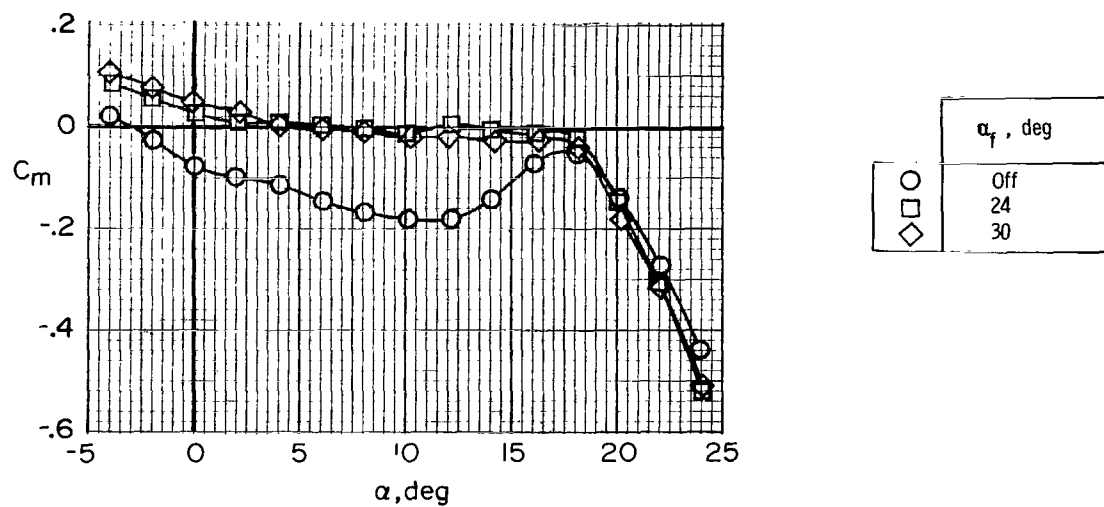
(b) Pitching-moment coefficient.

Figure 9.- Concluded.



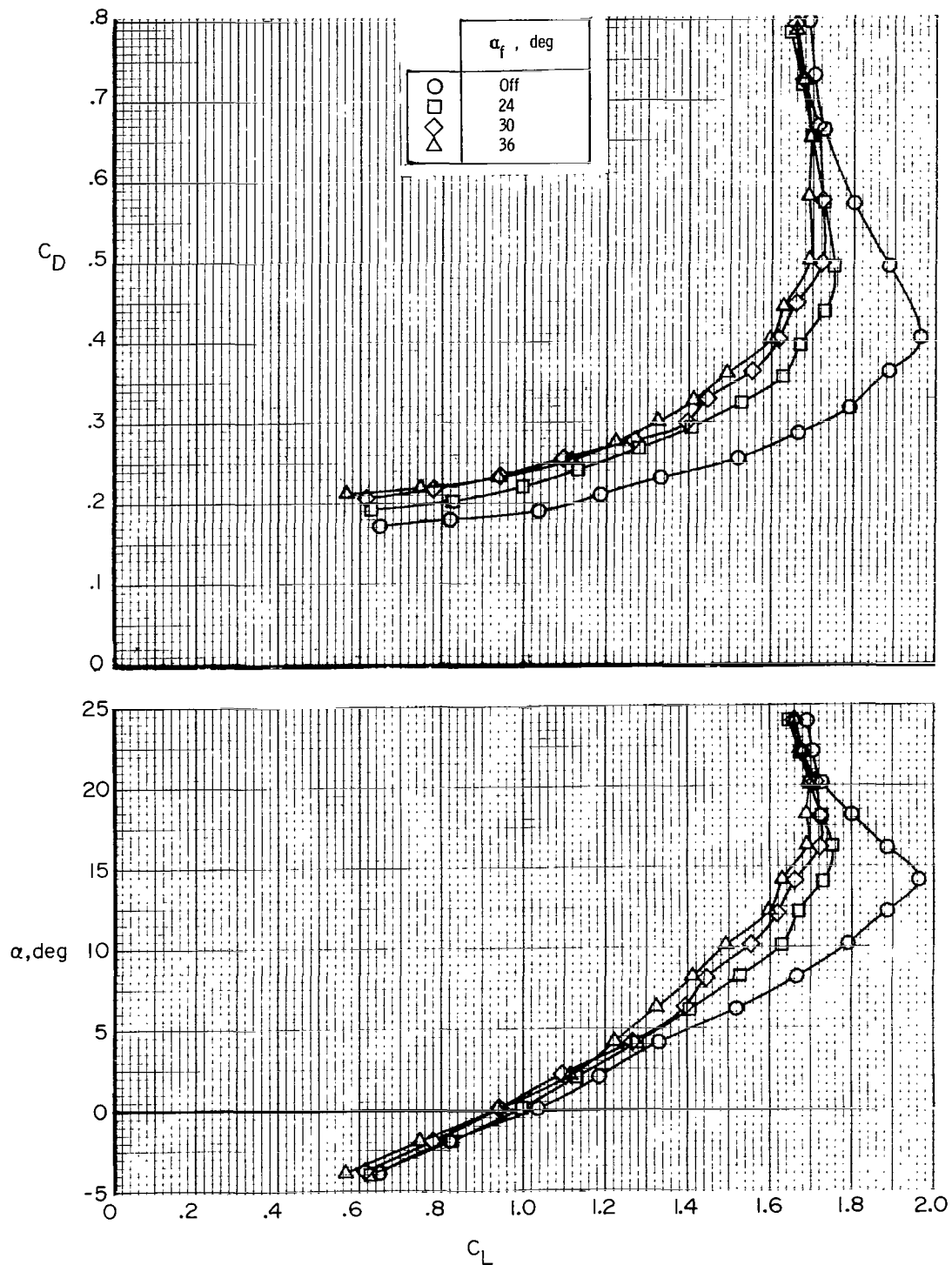
(a) Lift and drag coefficients.

Figure 10.- Effect of α_f of two fins on longitudinal aerodynamic characteristics of transport airplane model with the Clark Y airfoil fins located along 30-percent-chord line at $0.42b/2$ and $0.50b/2$. $i_t = 0^\circ$; landing flap configuration; landing gear down.



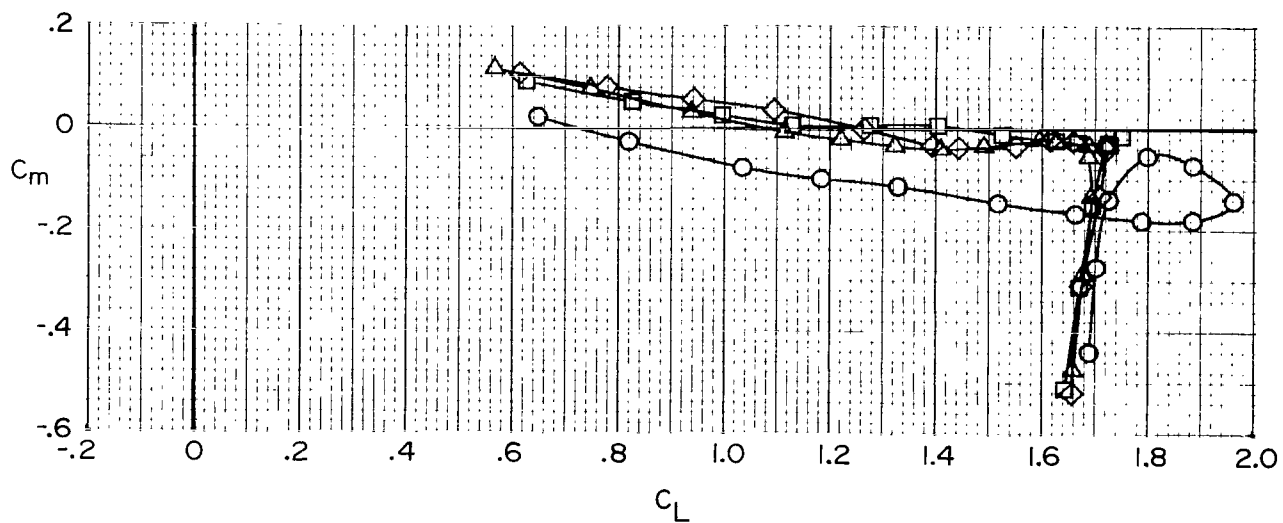
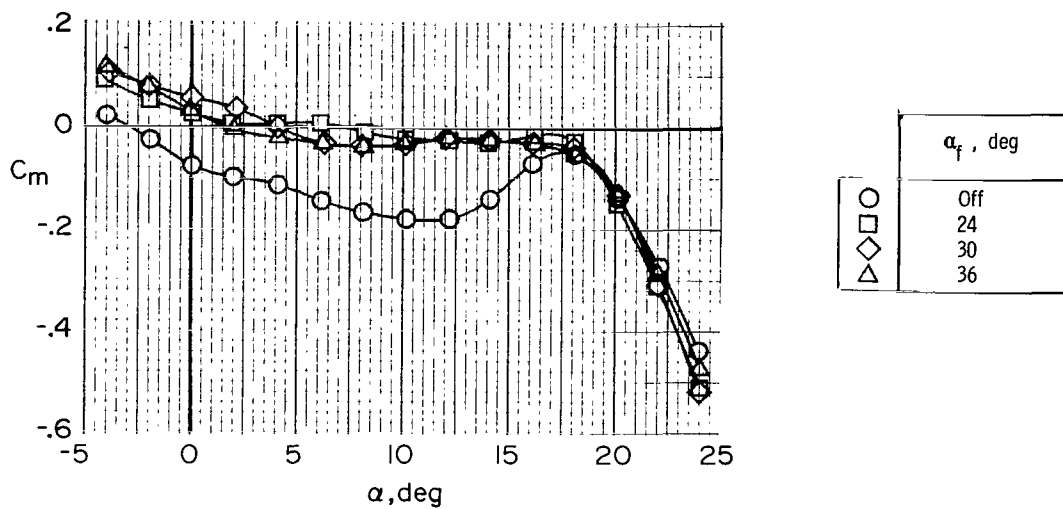
(b) Pitching-moment coefficient.

Figure 10.- Concluded.



(a) Lift and drag coefficients.

Figure 11.- Effect of α_f of two fins on longitudinal aerodynamic characteristics of transport airplane model with the Clark Y airfoil fins located along 30-percent-chord line at $0.46b/2$ and $0.53b/2$. $i_t = 0^\circ$; landing flap configuration; landing gear down.



(b) Pitching-moment coefficient.

Figure 11.- Concluded.

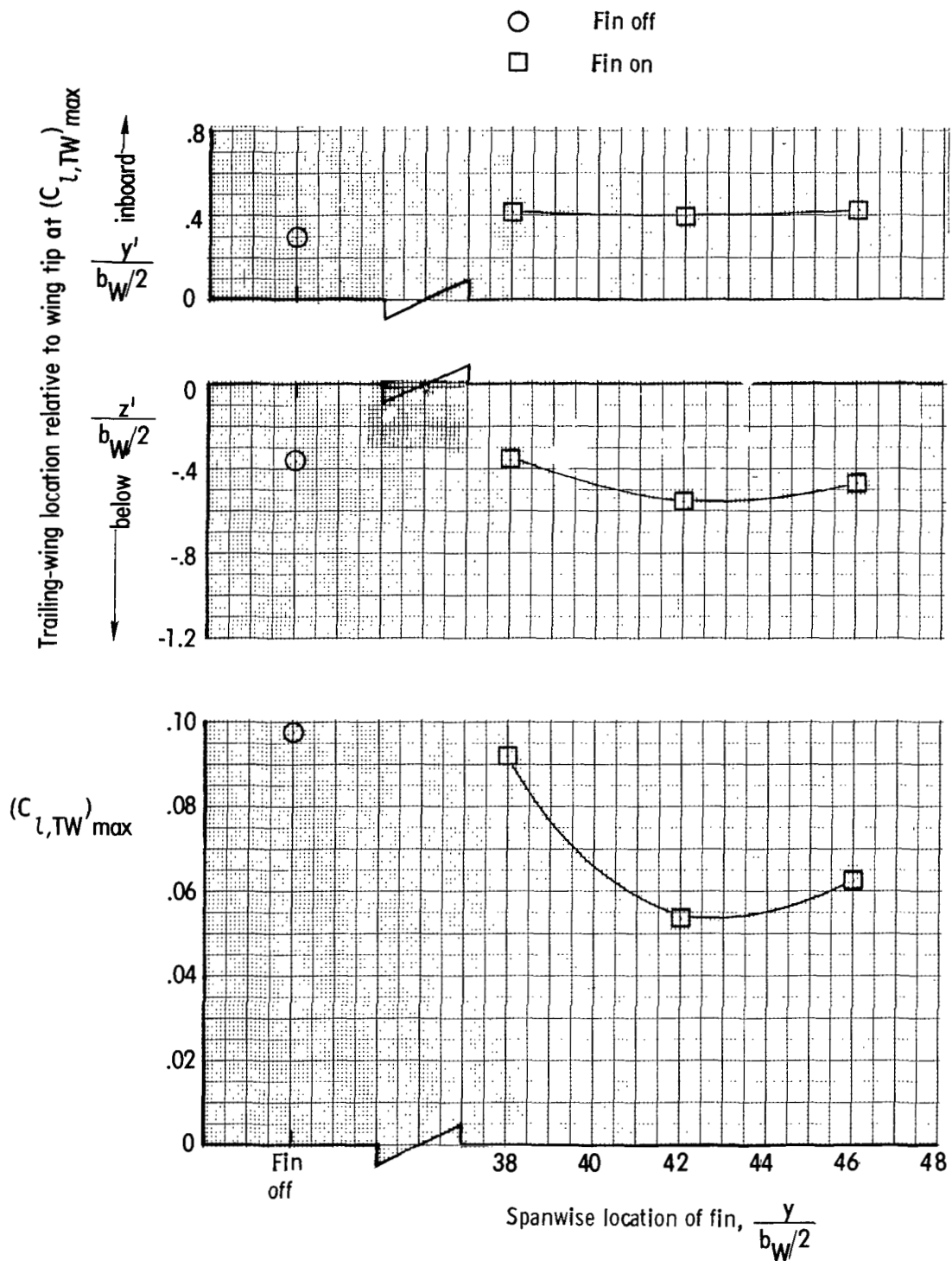


Figure 12.- Variation of trailing-wing location and rolling-moment coefficient with fin spanwise location for one Clark Y airfoil fin located along 30-percent-chord line at $\alpha_f = 30^\circ$. Trailing-wing model located 7.8 transport airplane model wing spans behind transport airplane model; $C_{L,trim} = 1.2$.

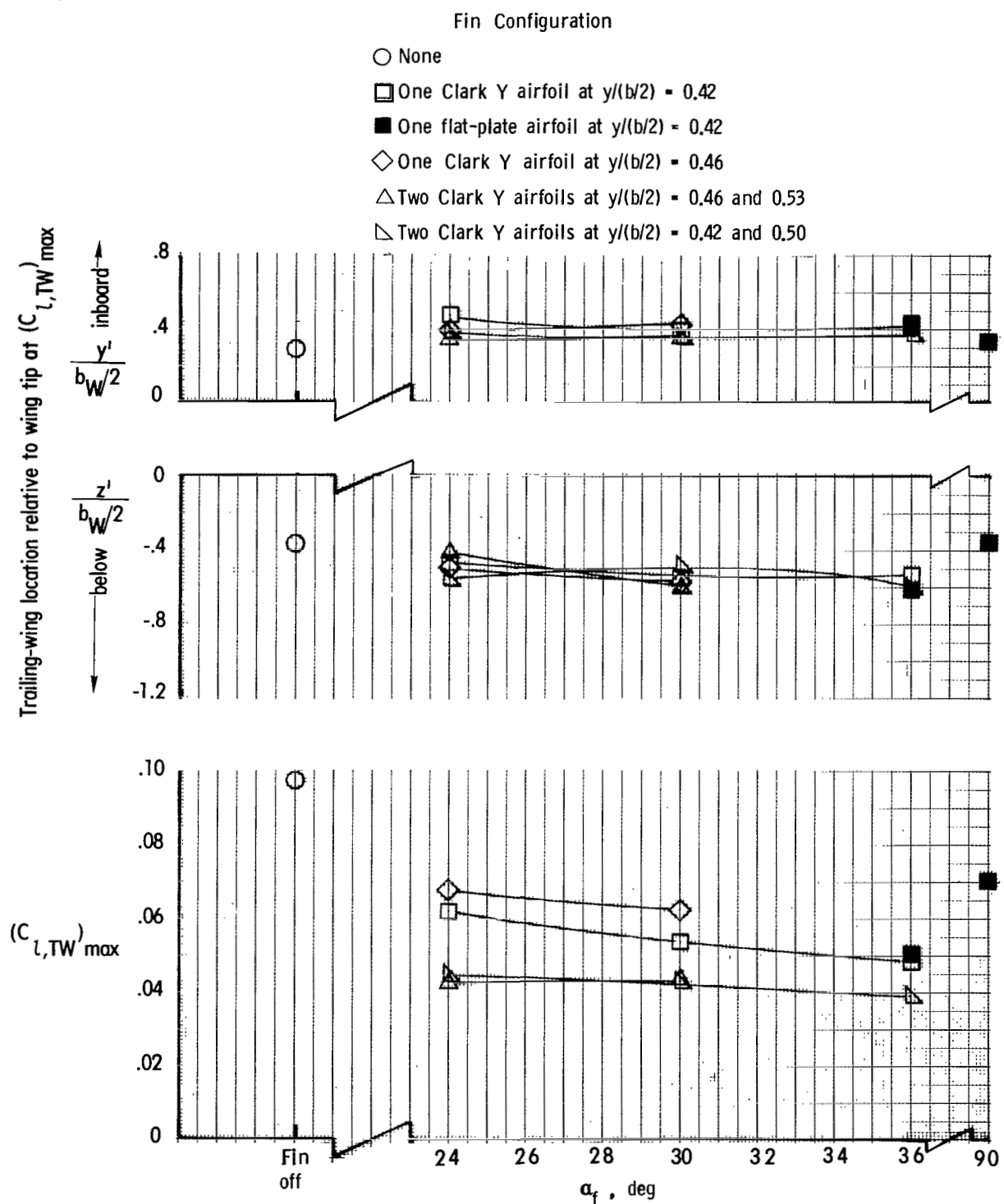


Figure 13.- Variation of trailing-wing location and rolling-moment coefficient with α_f for various fin configurations. Trailing-wing model located 7.8 transport model wing spans behind transport airplane model; $C_{L,trim} = 1.2$.

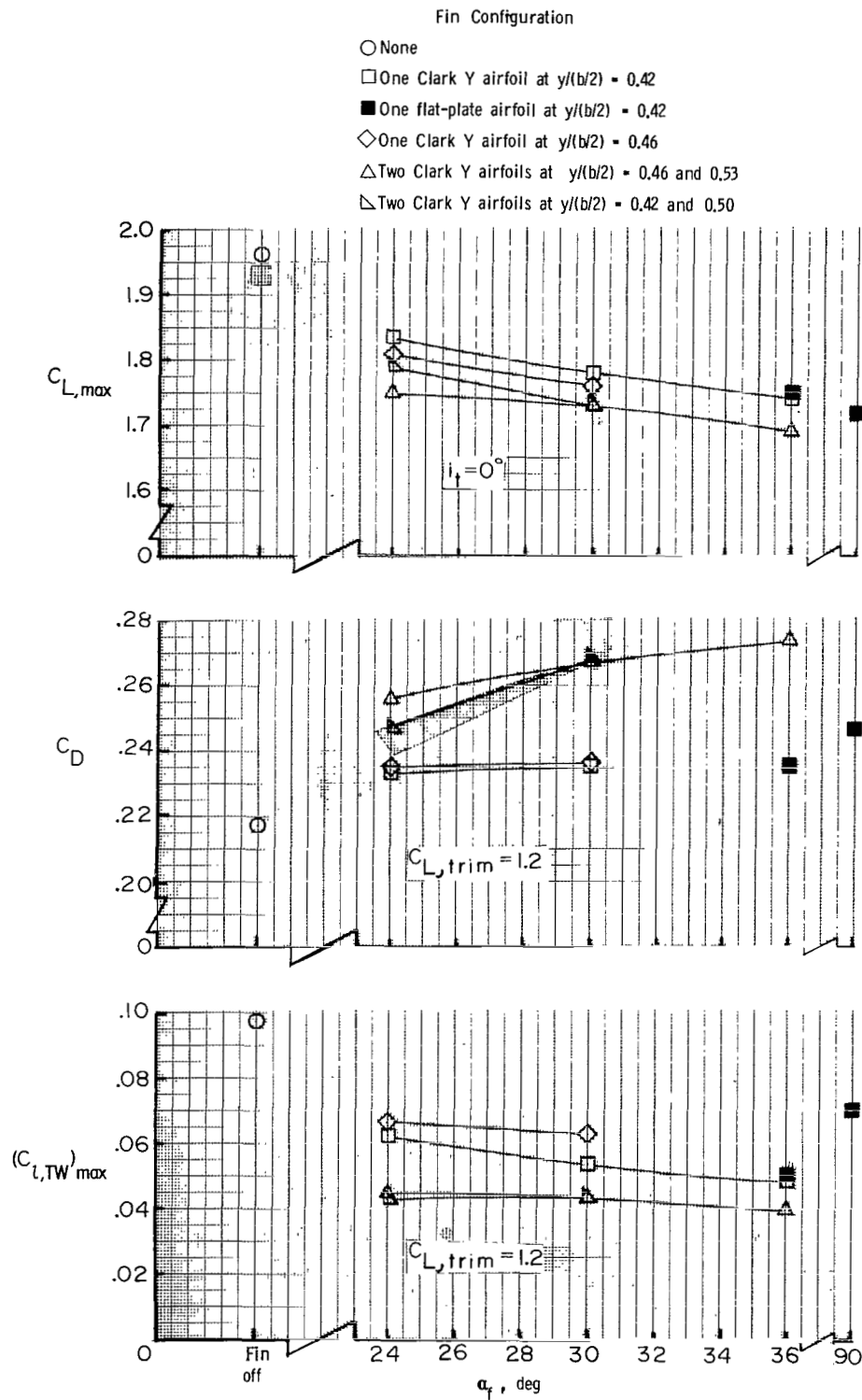


Figure 14.- Summary of reductions in maximum trailing-wing rolling-moment coefficient and penalties in drag and maximum lift obtained for various fin configurations. Trailing-wing model located 7.8 transport model wing spans behind transport airplane model.

1. Report No. NASA TP-1453		2. Government Accession No.		3. Recipient's Catalog No.	
4. Title and Subtitle LOW-SPEED WIND-TUNNEL INVESTIGATION OF WING FINS AS TRAILING-VORTEX-ALLEVIATION DEVICES ON A TRANSPORT AIRPLANE MODEL				5. Report Date June 1979	
7. Author(s) Delwin R. Croom and G. Thomas Holbrook				6. Performing Organization Code	
9. Performing Organization Name and Address NASA Langley Research Center Hampton, VA 23665				8. Performing Organization Report No. L-12776	
12. Sponsoring Agency Name and Address National Aeronautics and Space Administration Washington, DC 20546				10. Work Unit No. 514-52-03-02	
15. Supplementary Notes				11. Contract or Grant No.	
16. Abstract <p>An investigation was made in the Langley V/STOL tunnel to determine, by the trailing-wing sensor technique, the trailing-vortex-alleviation effectiveness of both a one- and a two-fin configuration (semicircular with a radius of 0.043 semi-span) on a jumbo-jet transport airplane model in its landing configuration. The fins were located on the upper surface of the transport model wing along the 30-percent-chord line. The fin configurations were effective in reducing the vortex-induced rolling moment, by amounts varying from 28 to 60 percent, on the trailing wing model located at a distance of 7.8 transport model wing spans downstream of the transport model.</p> <p>The flow over the fins and over the transport airplane model wing downstream of the fins was observed to be separated and turbulent. All fin configurations caused a reduction in maximum lift coefficient, a positive increment in drag coefficient, and an increment in nose-up pitching-moment coefficient on the transport airplane model.</p>				13. Type of Report and Period Covered Technical Paper	
17. Key Words (Suggested by Author(s)) Vortex alleviation Trailing-vortex hazard				14. Sponsoring Agency Code	
18. Distribution Statement Unclassified - Unlimited				Subject Category 02	
19. Security Classif. (of this report) Unclassified		20. Security Classif. (of this page) Unclassified		21. No. of Pages 28	
				22. Price* \$4.50	

National Aeronautics and
Space Administration

Washington, D.C.
20546

Official Business

Penalty for Private Use, \$300

THIRD-CLASS BULK RATE

Postage and Fees Paid
National Aeronautics and
Space Administration
NASA-451



1 1 1U, A, 060879 S00903DS
DEPT OF THE AIR FORCE
AF WEAPONS LABORATORY
ATTN: TECHNICAL LIBRARY (SUL)
KIRTLAND APB NM 87117

NASA

POSTMASTER:

If Undeliverable (Section 158
Postal Manual) Do Not Return